J Mater Sci (2023) 58:16474–16487

Metals & corrosion

Effect of hard plate rolling on microstructure and mechanical properties of Mg-9Al-1Zn-based composites reinforced with Ti-6Al-4V particles

Xin Cao[1,*], Bing Wu[1], Ming Liang[1], and Jianfeng Li[1]

[1] *Northwest Institute For Nonferrous Metal Research, Mg-Li Materials Research Institute, Xi'an, Shannxi 710016, People's Republic of China*

Received: 28 June 2023
Accepted: 13 October 2023
Published online: 5 November 2023

ABSTRACT

In this work, the TC4/AZ91 composites were fabricated through spark plasma sintering (SPS) followed by hard plate rolling (HPR) of a novel processing technology. The microstructure evolution and mechanical properties of the magnesium (Mg) matrix composites (MMCs) were investigated. The results illustrated that there were no other precipitates in TC4/AZ91 composites except for α-Ti and $Mg_{17}Al_{12}$ phases. The grains were refined significantly and TC4 particles occurred plastic deformation after a single pass via HPR, and the grain refinement of the TC4/AZ91 composites after HPR was attributed to TC4-induced particle-stimulated nucleation (PSN) mechanism and the pinning effect of fine $Mg_{17}Al_{12}$ phases. The deformable TC4 particles were beneficial to alleviate the stress concentration around them, resulting in dynamic recrystallization grain size around them being slightly smaller than relatively far away. Among them, the TC4/AZ91 composite with a thickness reduction of 70% by HPR exhibited favorable comprehensive mechanical properties: The yield strength (YS), ultimate tensile strength (UTS) and elongation (EL) were 206 Mpa, 349 Mpa and 7.9%, respectively. The superior mechanical properties were primarily ascribed to three aspects: (I) grain refinement, (II) the good interfacial bonding between Mg matrix and TC4 particles, and (III) the deformability of TC4 particles.

Introduction

Mg matrix composites (MMCs) have been attracting extensive attentions for structural applications owing to the lightweight [1–3], high specific strength [4] and superior damping capacities [5]. Generally, the selected reinforcements were mainly ceramic particles such as SiC [6], TiB_2 [7] and AlN [8]. Although nanoscale ceramic particles can enhance the strength effectively, they can deteriorate the ductility of MMCs due to physical differences between ceramic particles and Mg matrix such as crystal structure and the

Handling Editor: Megumi Kawasaki.

Address correspondence to E-mail: caoxin0819@126.com

https://doi.org/10.1007/s10853-023-09044-8

coefficient of thermal expansion [2, 9]. Recently, using metallic particles such as Ti, Ni and Fe reinforced MMCs while taking into account its strength and ductility [10]. Among them, Ti and its alloy particles were considered the most advantageous in improving strength and ductility simultaneously, because it was difficult to form brittle intermetallic compounds with Mg matrix to generate favorable influence on mechanical properties of matrix [11, 12]. Currently, there have been many studies on Ti- and its alloy particle-reinforced Mg alloys. Rashad et al. employed semi-powder metallurgy way to prepare the Mg-Ti and Mg-10Ti-1Al composites, and confirmed that the addition of Ti particles effectively improved the tensile strength and elongation [13]. Wang et al. confirmed that TC4/AZ91 composites exhibited better ductility compared to SiC/AZ91 composites [10]. The superior ductility of the TC4/AZ91 composites can be attributed to: (I) the similar crystal structure was beneficial to alleviate residual stresses in the composites, (II) the favorable interfacial bonding existed between Ti and Mg matrix owing to the better wettability and (III) the excellent ductility of TC4 particles was conducive to force transfer during plastic deformation. Based on the above outstanding advantages, it is necessary to further research on TC4-reinforced Mg alloys.

To date, various traditional methods such as powder metallurgy (PM) and stir casting were used to fabricate composite materials [14]. The stir casting can fabricate large and complex structural parts, but the problems such as reinforcements agglomeration and sedimentation greatly deteriorated composites comprehensive mechanical properties. Comparatively, PM method could realize uniform distribution of the reinforcements in the composites through mechanical mixing powders in advance [15]. However, the porosity of composites prepared by PM method greatly deteriorated the mechanical properties of composites. Therefore, the composites can be further optimized through secondary processing such as hot extrusion [10] and friction stir processing [16]. Roy et al. revealed that the composite microstructure was refined by hot extrusion effectively, and the degree of grain refinement was greater than that of the unreinforced alloys [17]. Dinaharan et al. fabricated TC4/AZ91 composites by hot-press sintering following by extrusion, which achieved good interfacial bonding between matrix and reinforcement particles to obtain favorable tensile properties (211 MPa, 303 MPa and 18.7%, respectively) [18]. At present, the TC4/AZ91 composites prepared by PM method were usually processed by hot extrusion, with little rolling deformation. Our previous experiment on SPS TC4/AZ91 composites secondary processing also suggested that the rolled plates cracked and formed penetrating cracks on the surface by conventional rolling (CR) method. The main reason was ascribed to that the large porosity of PM composites, while the CR shear force was too large along rolling direction to cause cracks between the reinforcements and Mg matrix. Therefore, a special secondary processing method was urgently needed to deform SPS TC4/AZ91 composites. Wang et al. proposed a novel secondary processing method of hard plate rolling (HPR) in the study of hard deformation Mg alloys [19]. The HPR method can decrease the force in rolling direction (RD) and increase the force in normal direction (ND) by adding cemented carbide plates on the upper and lower surface of sample. The experimental result proved that not only the SPS TC4/AZ91 composites can be deformed by HPR, but also achieved large thickness reduction (~90%). Currently, there were very rare works focusing on the HPR effect on microstructure evolution and mechanical performance of SPS TC4/AZ91 composites. In particular, the grain size, texture strength and interfacial bonding caused by HPR have not been thoroughly studied. Therefore, it is very worthwhile to investigate the relationship between the microstructure and mechanical properties of the SPS TC4/AZ91 composite through HPR secondary processing.

The purpose of this work is to clarify the strengthen and ductility mechanism of TC4/AZ91 composites after HPR deformation by studying the microstructure evolution. Meanwhile, the influence of the deformable TC4 particles on the microstructure evolution and mechanical mechanism of the TC4/AZ91 composites is further discussed.

Experimental details

Preparation of composites

Commercial AZ91 powders with average size of ~56 μm and TC4 powders with average size of ~43 μm were used to fabricate TC4/AZ91 composites (as shown in Figure S1). Firstly, AZ91 powders and TC4 powders were mechanically mixed in an agate mortar for 30 minutes in a glove box under pure argon atmosphere to ensure uniform powder mixing (Fig. 1a). The

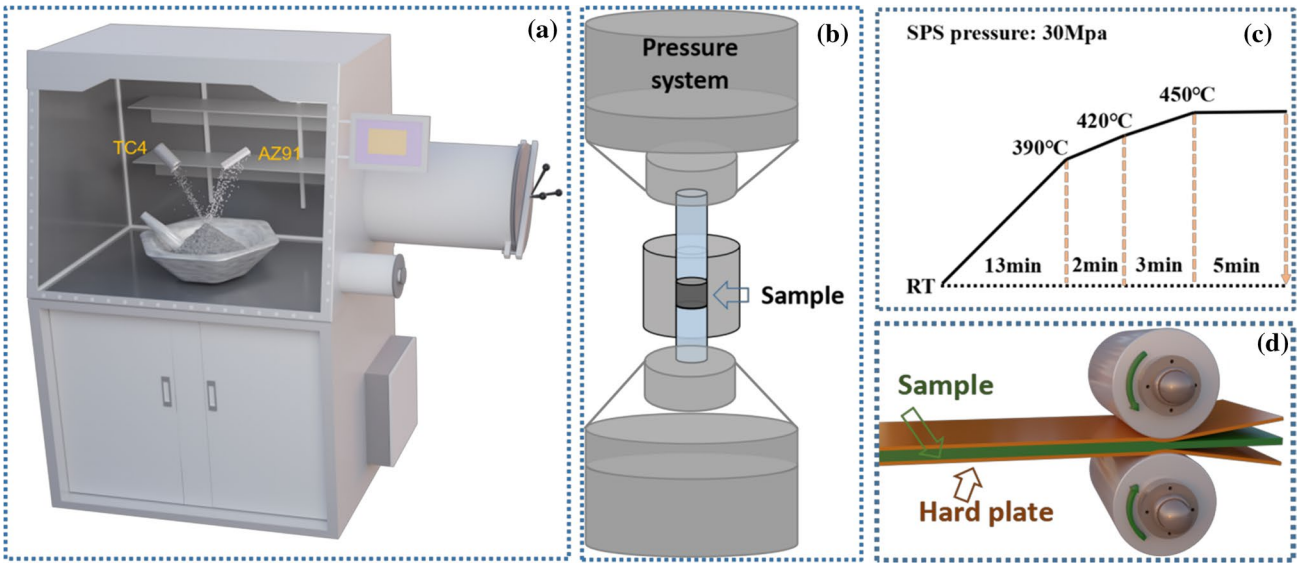

Figure 1 **a** Manual powder mixing glove box, **b** spark plasma sintering furnace, **c** detailed sintering process flow and **d** process of hard plate rolling.

mass percentage of TC4 particles in AZ91 alloys in this work is 10%. Secondly, the mixed TC4/AZ91 powders were fabricated by spark plasma sintering (SPS, Fig. 1b). The mixed powders were sintered at constant pressure of 30 MPa to obtain samples with a height of 10 mm and a diameter of 30 mm. (The detailed process is shown in Fig. 1c.) Finally, the SPS samples were cut into plates with dimensions of 25 mm×10 mm×6 mm and used for hard plate rolling (HPR). Select 0.5-mm-thick steel plate as the hard plate, grind the sample to 3000-grit using SiC abrasive papers and fix it between the two hard plates, as shown in Fig. 1d. Before rolling, the specimens were preheated at 450 °C for 15 min (the roll was not heated), and the rolling speed was 250 mm s^{-1}, with a thickness reduction of ~60%, ~70% and ~80%, respectively, by a single pass via HPR method.

Microstructure characterization and mechanical tests

Phase constitutions were detected by X-ray diffraction (XRD, D/MAX-1200) with Cu Kα radiation. The microscopic morphology was observed by field emission scanning electron microscope (SEM, JEOL JSM-7800F) equipped with a backscattered electron (BSE) detector. The samples for SEM observation were grinded, polished and etched. (The ingredients of etchant were 5 ml acetic acid+5.5 g picric acid+10 ml H_2O+90 ml ethanol.) The average size of TC4/AZ91 composites was counted by Nano Measurer 1.2 software based on the SEM results. The transmission electron microscopy (TEM, JEM-2100Plus) was used to observe nano-precipitated phase, dislocation density and ultrafine grains. The samples were prepared by grinding and electro-polished with an AC2 solution at 20 V for 120 s for electron backscattered diffraction (EBSD, the ingredient of AC2 was listed in Table S1). EBSD was performed at an accelerating voltage of 20 kV and a step size of 0.35 μm. The EBSD data were collected using AZtec software and analyzed by Channel 5 software to characterize grain orientations, grain sizes and micro-textures. In addition, the mechanical test was performed through a universal testing machine (UTM5105) at room temperature (tensile rate of 0.2 mm/min).

Results

Microstructure analysis

Figure 2 depicts the X-ray diffraction patterns (XRD) of TC4/AZ91 composites after HPR with different thickness reduction. All the samples have the peaks associated with α-Ti, which is ascribed to the addition of TC4 particles in AZ91 alloys. The diffraction peak of $Mg_{17}Al_{12}$ phase only appears in rolled TC4/AZ91 composites, and the diffraction peak intensity gradually decreases with the increase in the thickness

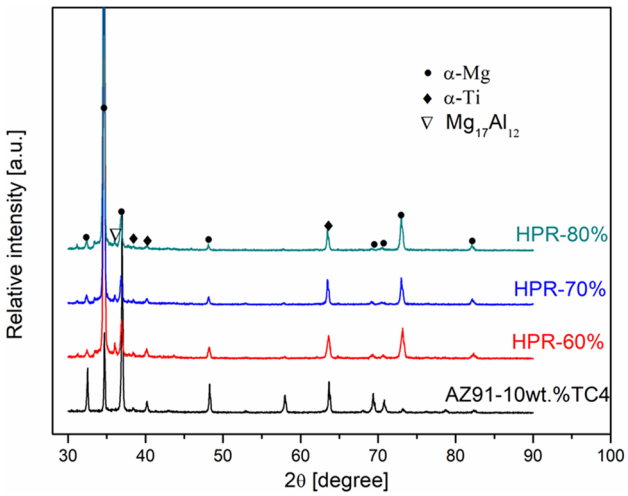

Figure 2 XRD patterns of sintered and hard plate rolling TC4/AZ91 composites.

reduction from ~60 to ~80%. In addition, there are no peaks of other intermetallic compounds detection, as shown in Fig. 2, demonstrating that the TC4 particles do not have metallurgical reaction with the AZ91 matrix. Previous work revealed that the Al present in AZ91 alloys easily tends to react with Ti element to formation of brittle Al_3Ti phases [20]. It shows that there is no Al_3Ti phase formation in the SPS and HPR TC4/AZ91 composites (Fig. 2), which is ascribed to the lower sintering temperature and shorter reaction duration. Furthermore, the peak intensity of (0001) plane is significantly enhanced and (10–11) peak is weakened with the increase in the thickness reduction, which indicates that stronger basal texture appears in RD–TD plane after rolling.

Figure 3 exhibits the backscatter electron (BSE) images of the TC4/AZ91 samples after HPR with different thickness reduction to show the TC4 particles and precipitated phases distribution. It is evident that the near-spherical TC4 particles (marked with white arrows) are randomly distributed in MMCs without cluster. The finely distributed particles (marked with yellow arrows) are confirmed as $Mg_{17}Al_{12}$ phases by energy-dispersive analysis (EDS), and no other new phases are clearly found. In addition, the length–diameter ratio of TC4 particles increases with the increase in the thickness reduction from 60 to 80%, which indicates that the TC4 particles in MMCs undergo plastic deformation during HPR. Wang et al. also observed that TC4 particles deformed and the length–diameter ratio was evidently increased after hot extrusion

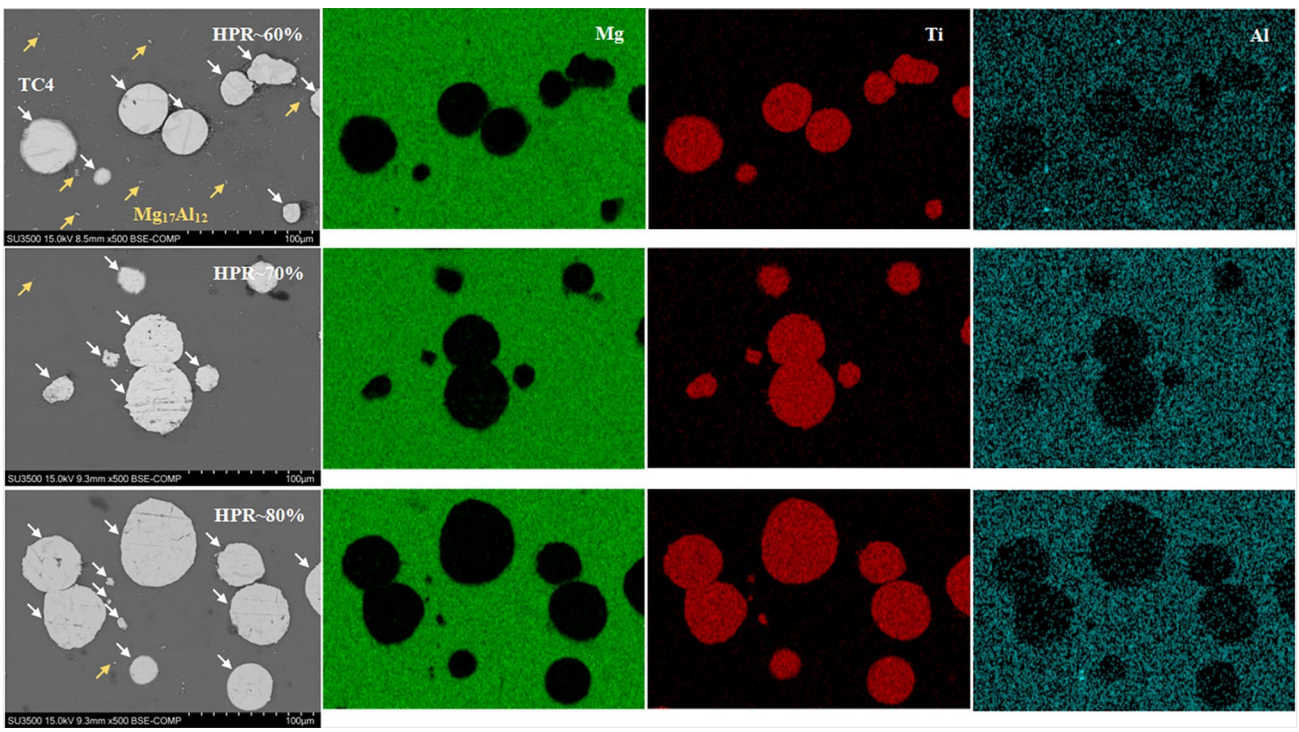

Figure 3 Surface scanning distribution of backscattered electron maps of HPR TC4/AZ91 composites with different thickness reduction.

[10]. These deformed TC4 particles are beneficial to coordinate the strength and ductility of composites, because it can effectively weaken the stress concentration around TC4 particles in MMCs.

Figure 4 shows the EBSD maps of TC4/AZ91 composites after HPR deformation. Noticeably, it reveals that the grain size of HPR composites first decreases rapidly and then slightly increases with the thickness reduction from 60% to 80%, and the values are estimated to be ~32.87 μm, ~7.75 μm and ~9.78 μm, respectively. Simultaneously, we notice that the grain size of composites around TC4 particles is slightly smaller than those away from particles, and the trend of grain size variation is counted in Fig. 4. (The statistical method for grain size variation is shown in Fig. 4c, where the size of six grains is measured along different arrow-marked directions.) This phenomenon is slightly different from the grain size changes of conventional ceramic particles such as SiC-reinforced MMCs, in which the grains near the reinforcement particles are much finer than those away from reinforcement [21]. The reason for this discrepancy is mainly ascribed to the deformability of TC4 particles compared to hard ceramic particles. The corresponding inverse pole figure (IPF) and pole figure (PF) of rolled TC4/AZ91 composites are shown in Fig. 5, revealing that the intensity of basal texture is decreased along with the increase in the thickness reduction, and the value are estimated to be 13.68, 7.84 and 6.12, respectively. The main reason for texture weakening is attributed to dynamic recrystallization (DRX) caused by increased deformation [22].

Figure 6 shows the TEM microstructure of the TC4/AZ91 composite after HPR with thickness reduction of

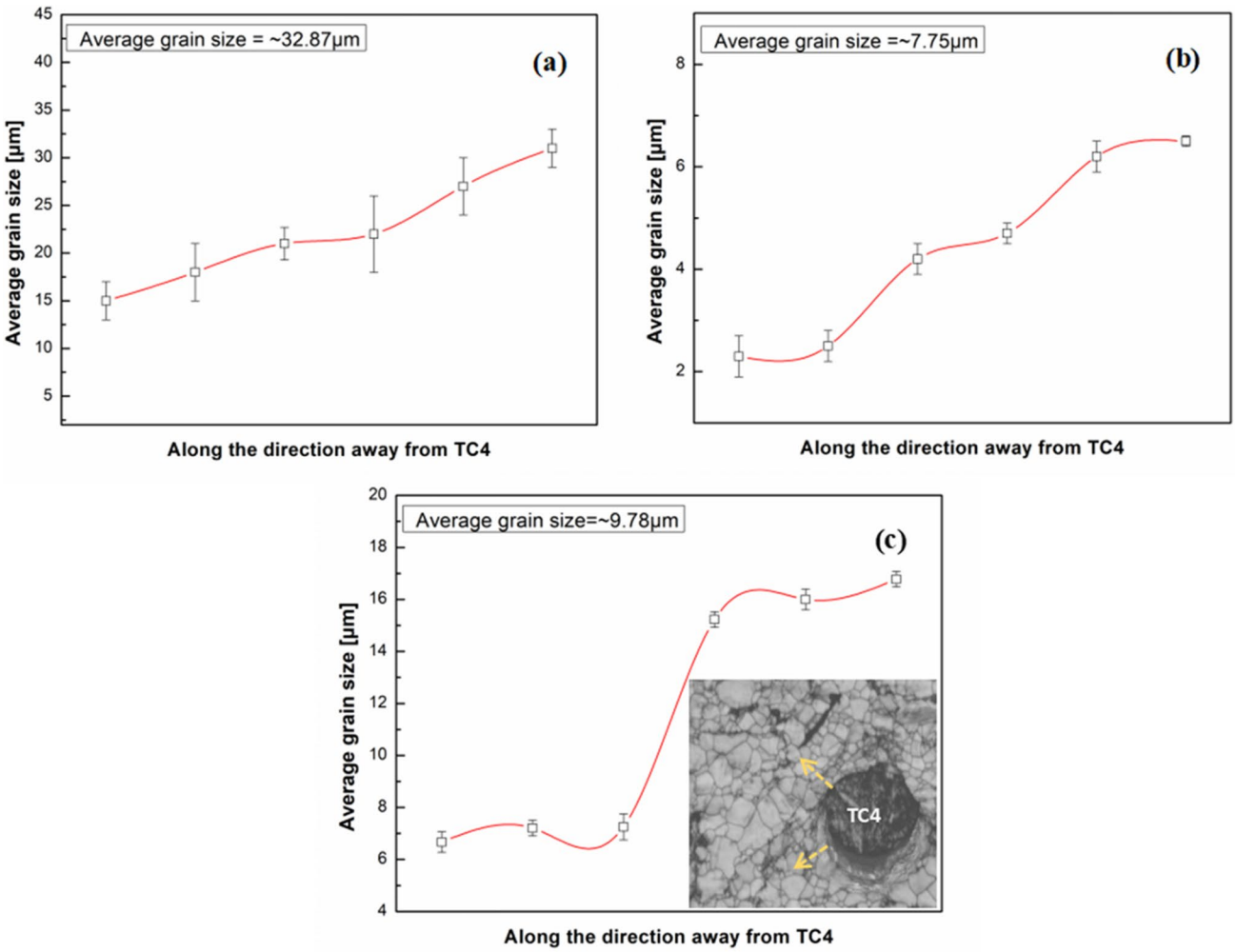

Figure 4 Statistics of grain size variation perpendicular to the direction of TC4 particles and average grain size of TC4/AZ91 composites after HPR with thickness reduction of 60%, 70% and 80%.

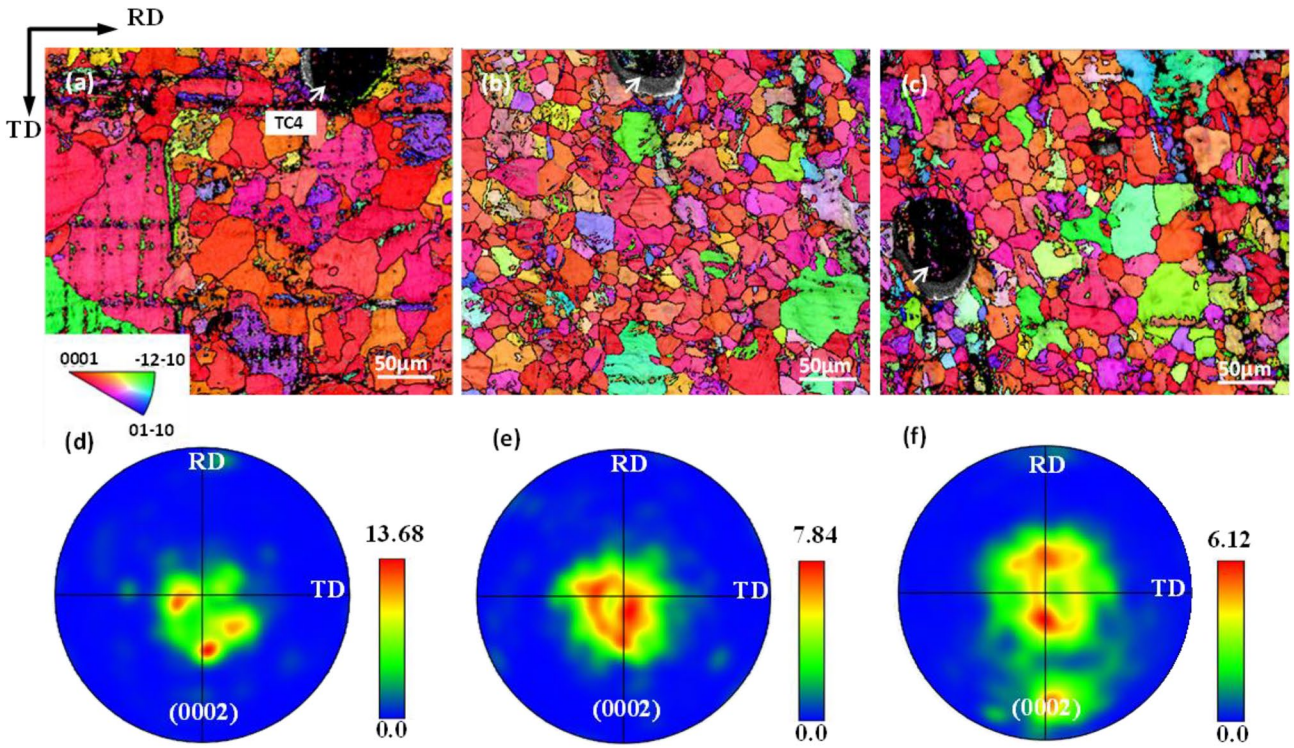

Figure 5 Electron backscatter diffraction (EBSD) maps of the TC4/AZ91 composites after HPR with different thickness reduction: **a**, **d** thickness reduction of 60%, **b**, **e** thickness reduction of 70% and **c**, **f** thickness reduction of 80%.

70%. Figure 6a shows that the areas around small TC4 particles are rich in high-density dislocations, which will promote dynamic recrystallization nucleation through particle-stimulated nucleation (PSN) mechanism, resulting in smaller grain size near TC4 particles. Figure 6b, c shows the fine dispersed $Mg_{17}Al_{12}$ phase of 200~300 nm precipitated along grain boundary (GBs) and the low-density dislocation appears around the precipitated $Mg_{17}Al_{12}$ phase. The corresponding diffraction pattern of $Mg_{17}Al_{12}$ phase marked by yellow arrow is shown in Fig. 6b. These dispersed $Mg_{17}Al_{12}$ phases have pinning effect at GBs to hinder dislocation slip and restrict grain growth. Wang et al. confirmed that the finer and dispersed particles precipitated at GBs can optimize the reinforced efficiency and weaken the stress concentrations to enhance both the strength and ductility of the composites [21]. In addition, Fig. 6d shows the ultrafine grain morphology after HPR, with the average grain size of ~1 μm.

Mechanical properties

Figure 7 exhibits the tensile stress–strain curves of TC4/AZ91 composites before and after HPR, and the corresponding mechanical property (YS, UTS and EL) results are listed in Table 1. Compared with SPS TC4/AZ91 composites, the comprehensive mechanical properties of the MMCs are drastically improved by HPR. The YS, UTS and EL increase from ~120 MPa, ~212 MPa and ~3.9% of SPS TC4/AZ91 composite to ~206 MPa, ~349 MPa and ~7.9% after HPR with thickness reduction of ~70%, respectively. HPR method can sensibly improve the comprehensive mechanical properties of the composites. In particular, the YS and EL are nearly doubled. Making a comparison of this work with other particle-reinforced AZ91 composites, the corresponding results are listed in Table 2. Compared with the conventional ceramic particles, i.e., SiC [25, 26], TiB [27], etc., reinforced MMCs, the TC4 particles in MMCs can not only effectively improve its strength, but also maintain good ductility.

Figure 8 shows the tensile fracture morphology of HPR TC4/AZ91 composites. For HPR composites with a thickness reduction of 60%, the fracture surface appears two kinds of dimples, the larger dimples are caused by TC4 particles falling off and the finer dimples are formed by fracture of Mg matrix. Meanwhile, TC4 particles are noticed inside the dimples,

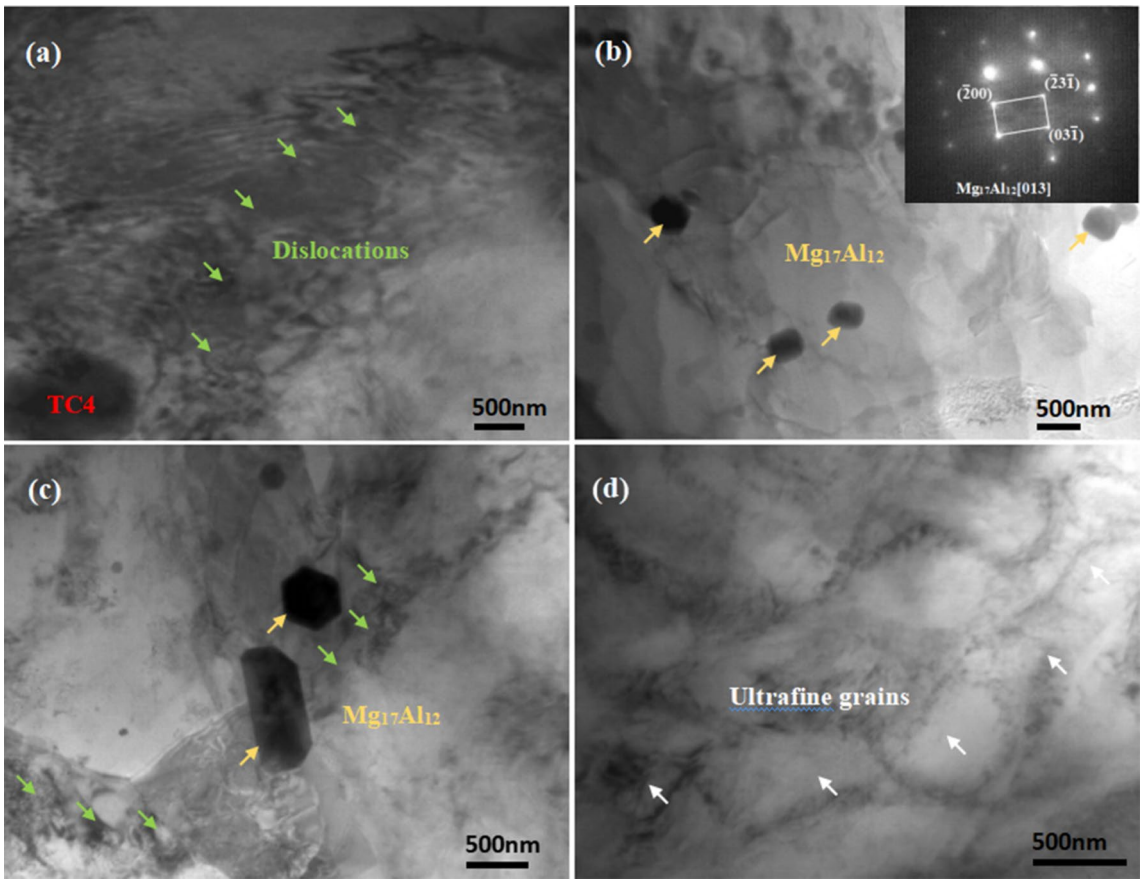

Figure 6 Transmission electron microscopy (TEM) maps of TC4/AZ91 composites after HPR with thickness reduction of 70%: **a** TC4 particles and high-density dislocation; **b** nanoscale $Mg_{17}Al_{12}$ precipitate pinning GBs and corresponding diffraction patterns of $Mg_{17}Al_{12}$ precipitate marked by yellow cross; **c** $Mg_{17}Al_{12}$ precipitates and dislocation tangle zones; **d** microstructure of the fine-grained (FG) regions.

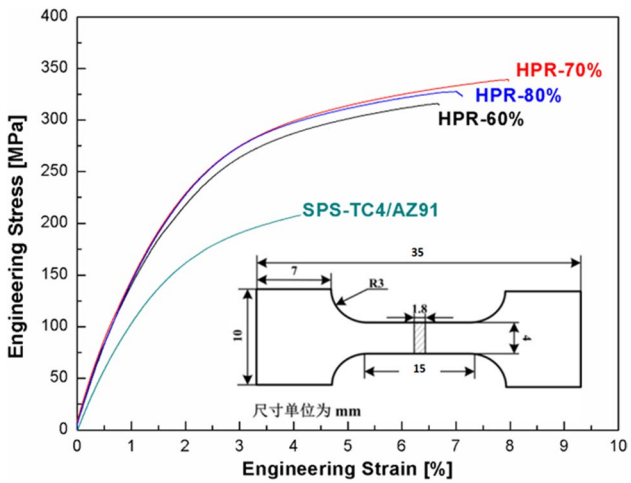

Figure 7 Engineering stress–strain curve of TC4/AZ91 composites at room temperature.

Table 1 Tensile properties of spark plasma sintered (SPS) TC4/AZ91 composites and TC4/AZ91 composites after HPR deformation with a thickness reduction of 60%, 70% and 80%

Samples	Yield strength (YS), $\sigma_{0.2}$/MPa	Ultimate tensile strength (UTS), σ_b/MPa	Elongation (EL), δ_p/%
SPS	120^{+3}_{-3}	212^{+2}_{-4}	$3.9^{+0.3}_{-0.8}$
HPR~60%	184^{+7}_{-4}	315^{+4}_{-7}	$6.7^{+0.6}_{-1.0}$
HPR~70%	206^{+3}_{-4}	349^{+3}_{-5}	$7.9^{+0.4}_{-0.7}$
HPR~80%	205^{+7}_{-5}	327^{+9}_{-2}	$7.1^{+0.6}_{-1.2}$

suggesting that the break is mainly induced by interfacial division between TC4 particles and AZ91 matrix. The obvious interface fracture appears between AZ91 matrix and TC4 particles (as shown in Fig. 8a). Further with the increase in the thickness reduction to

Table 2 Tensile properties of TC4/AZ91 composites and Mg matrix composites reinforced by other ceramic particles

Materials	YS(MPa)	UTS(MPa)	EL(%)
AZ91 cast [10]	85	143	3.9
AZ91-10 wt.% TC4 SPS [this work]	120	212	3.9
AZ91-10 wt.% TC4 HPR-60% [this work]	203	323	5.9
AZ91-10 wt.% TC4 HPR-70% [this work]	206	349	7.9
AZ91-10 wt.% TC4 HPR-80% [this work]	184	315	6.8
AZ91-10 wt.% TC4 cast [21]	125	245	3.9
AZ91-10 wt.% TC4 as-extruded [23]	249	369	6.4
AZ91-5 vol.%Ti_2AlC cast [24]	108	200	3.4
AZ91-10 vol.%SiC cast [25]	120	135	0.47
AZ91-10 vol.%SiC as-extruded [26]	247	350	4.0
AZ91-2.5 wt.%TiB_2 cast [27]	121	207	6.8

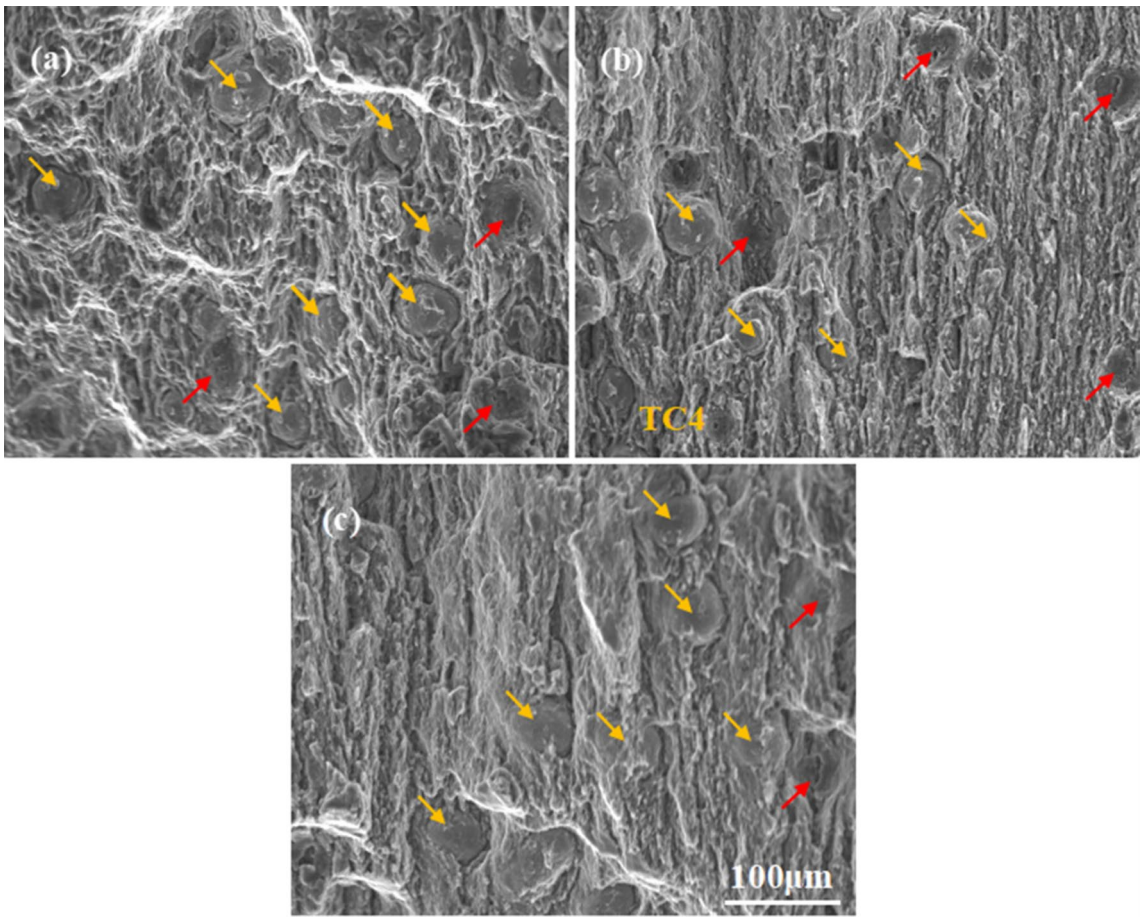

Figure 8 Scanning electron microscope (SEM) images of the fractured surface of TC4/AZ91 composites after HPR with thickness reduction: **a** 60%, **b** 70% and **c** 80%.

~70% and ~80% by HPR deformation, the interfacial division between TC4 particles and matrix is seldom observed on the fracture surface, as shown in Fig. 8b, c. This phenomenon further proves that increasing the deformation by HPR can effectively improve the interfacial adhesion strength between TC4 particles and AZ91 matrix, thus avoiding interface aging to enhance the strengthening efficiency of reinforcements.

Discussion

Grain refinement analysis

Previous work illustrated that nucleation and growth of dynamic recrystallization (DRX) grains in present samples are related to two competing factors during rolling, i.e., driving force stored around coarse TC4 particle-stimulated nucleation (PSN) and Zener pinning pressure originated from dispersed $Mg_{17}Al_{12}$ at grain boundary (GBs) inhibits DRX grain growth [28]. Wang et al. also demonstrated that when the particles size of the reinforcement was greater than 1 μm, it would act as a favorable nucleation site to promote nucleation through PSN mechanism [21]. It is known to all that the hard reinforcement particles in composites can immensely inhibit matrix flow during deformation, resulting in stress concentration around them. Stress concentration induces high-density dislocations and large orientation gradients around those reinforcement particles, leading to the formation of particle deformation zones (PDZs). These PDZs will be favorable for DRX to occur in MMCs. That is to say, those hard reinforcement particles can effectively promote DRX nucleation and induce the formation of fine DRX grains during deformation. In Fig. 6, the TEM morphology confirms the formation of high-density dislocations around TC4 particles, and some near-spherical $Mg_{17}Al_{12}$ phases of 300–500 nm precipitate along GBs. This phenomenon further illustrates that the refinement effect of TC4 particles through the PSN mechanism and the pinning function of fine $Mg_{17}Al_{12}$ phases jointly promote the grain refinement of the TC4/AZ91 composites after HPR deformation.

In addition, Fig. 9 shows the detailed misorientation angles of GBs near TC4 particles. According to the recrystallization theory, the regions surrounding the coarse reinforcement particles are favorable for storing high distortion energy, which will preferentially become recrystallization nucleation sites. Figure 9c shows that the GBs near TC4 particles have a large misorientation angles, and the most GBs of fine-grained misorientation angles are between 20°~50°. Moreover, as the distance away from the TC4 particles increases, the misorientation angle of GBs gradually decreases. In Fig. 9c, the PSN almost promotes the completion of dynamic recrystallization and forms fine recrystallized grains. The deformation region is consumed by the nucleation and growth of recrystallization grains. This result further reveals that TC4 particles play an crucial role in inducing DRX process and hence promoting the grain refinement (Fig. 10).

Mechanical property analysis

The improvement of comprehensive mechanical properties of TC4/AZ91 composites after HPR is ascribed to these reasons of microstructure refinement, high-strength TC4 particles as well good interface bonding between TC4 particles and AZ91

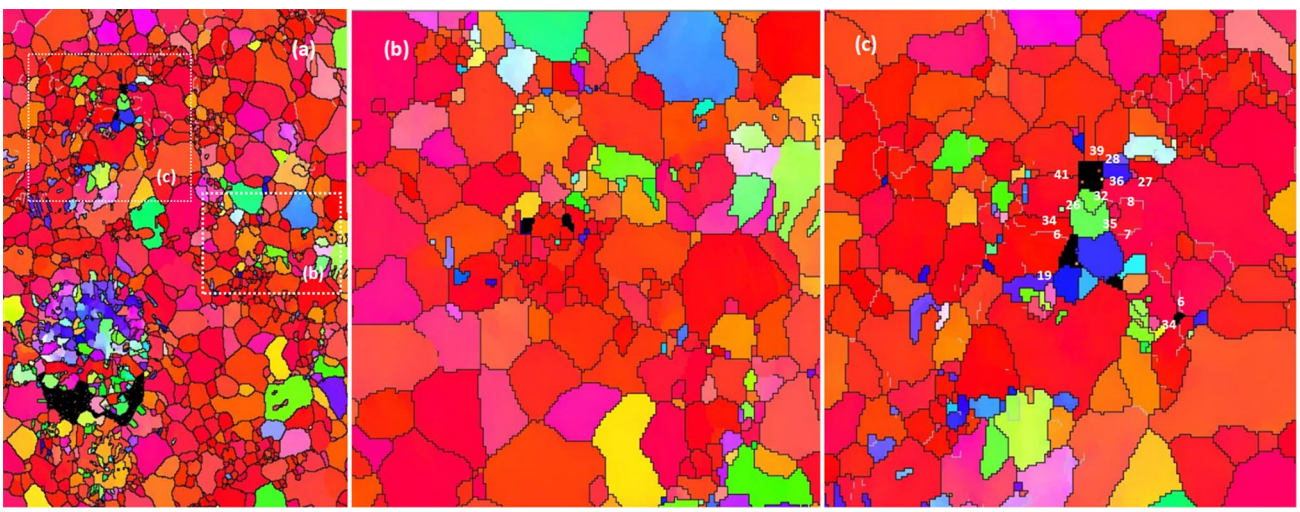

Figure 9 **a** EBSD orientation maps (in degrees) showing evidences of PSN induced by TC4 particles and **b** completed recrystallization, **c** misorientations (in degrees) of selected GBs around TC4 particles.

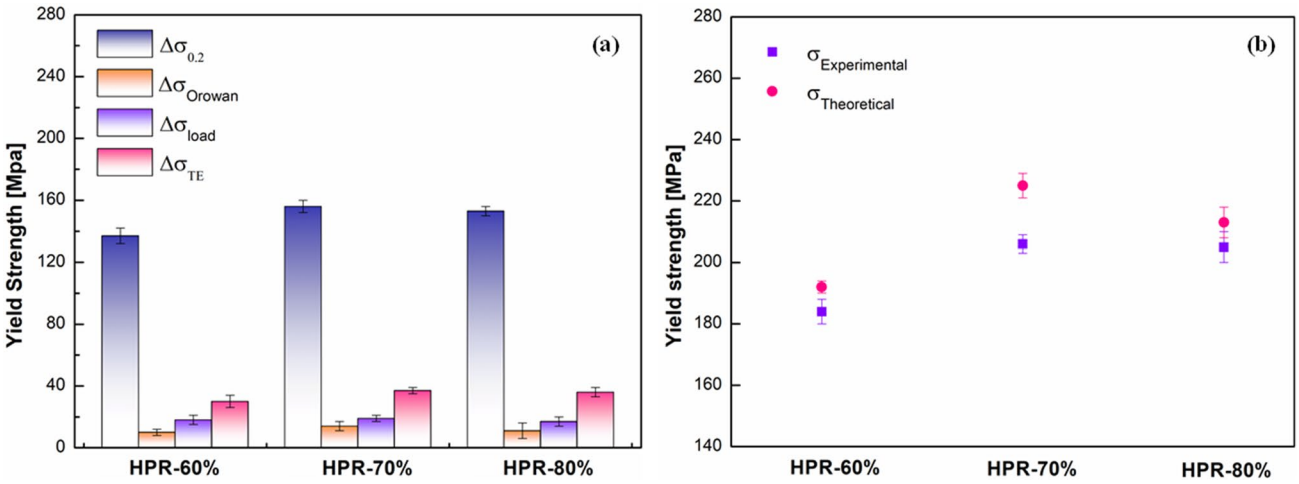

Figure 10 **a** Theoretical YS value of the different strengthening mechanisms in theoretical and **b** comparison of theoretical YS and experimental YS.

matrix. Therefore, the possible strengthening mechanisms of TC4/AZ91 composites are as follows: fine grain strengthening, dislocation multiplication strengthening, load transfer strengthening and Orowan strengthening. The microstructure of the TC4/AZ91 composites is significantly refined by HPR deformation, resulting in increased strength. The YS enhancement of MMCs through grain refinement is expressed by Hall–Petch equation [29]:

$$\Delta\sigma_{0.2} = k\left(d_c^{-\frac{1}{2}} - d_m^{-\frac{1}{2}}\right) \tag{1}$$

The k is Hall–Petch coefficient of matrix (~ 0.13 MPa $m^{1/2}$). d_m and d_c are the average grain size of the TC4/AZ91 composites before and after HPR deformation, respectively.

Then, considering the effect of load transfer when stress is transferred from the AZ91 matrix through the interfacial bonds to the TC4 particles, the YS enhancement through load transfer effect is expressed by the following equation [30]:

$$\Delta\sigma_{\text{load}} = 0.5f\sigma_{TC4/AZ91} \tag{2}$$

where f is the volume fraction of TC4 particles and the $\sigma_{TC4/AZ91}$ is yield strength of SPS TC4/AZ91 composites.

Third, considering the dislocation multiplication strengthening caused by thermal expansion difference between TC4 and AZ91 matrix, the YS improvement through mismatch of thermal expansion is expressed by the following equation [31]:

$$\Delta\sigma_{TE} = \sqrt{3}\varphi Gb\sqrt{\frac{12f\Delta C\Delta T}{(1-f)bd_p}} \tag{3}$$

where φ is geometric constant (~1.25). G is shear modulus (~1.66×10^4). b is Burger vector (~0.35). ΔC and ΔT are thermal expansion coefficient and temperature difference between rolling and testing, respectively. The d_p and f are diameter and volume fraction of TC4, respectively.

Lastly, considering the hinder effect of uniformly dispersed TC4 particles in MMCs by Orowan mechanism, the YS enhancement through Orowan is expressed by the following equation [30]:

$$\Delta\sigma_{\text{Orowan}} = \frac{\beta Gb}{d_p}\left(\frac{6f}{\pi}\right)^{1/3} \tag{4}$$

The β is a constant (~2). Other parameters are consistent with the above definition. Therefore, the total theoretical value of YS can be expressed through the following equation [31]:

$$\sigma_{\text{theoretic}} = \sigma_0 + \Delta\sigma_{0.2} + \Delta\sigma_{\text{load}} + \Delta\sigma_{TE} + \Delta\sigma_{\text{Orowan}} \tag{5}$$

Figure 11 depicts the contribution ratio of main strengthening factors to YS and the comparison between theoretical YS and experimental YS. According to Fig. 11a, the fine grain strengthening accounts for ~70% of the total theoretical YS contribution value, suggesting that dominate strengthening mechanism is fine grain strengthening in TC4/AZ91 composites after HPR. Normally, the finer the grain size is, the

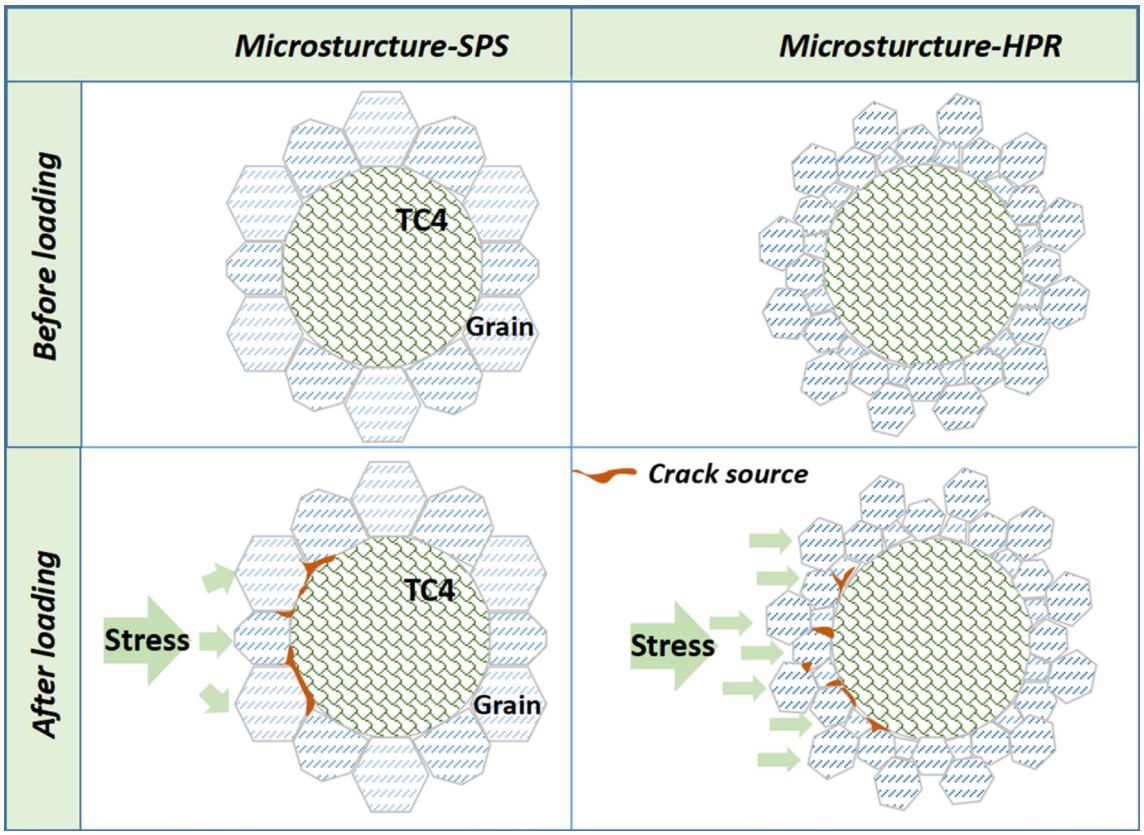

Figure 11 Schematic of stress distribution around TC4 particles during loading.

more significant the contribution to the YS of the composites [16]. Figure 4 shows that the grain size of TC4/AZ91 MMCs through HPR is significantly refined, and the refinement degree increases with the thickness reduction from 60 to 80%. The refined grains are beneficial for increasing dislocation slip resistance at GBs, which will greatly beneficial for enhancing strength of MMCs. Secondly, thermal mismatch reinforcement plays another significant factor. Because of the difference thermal expansion coefficient of TC4 particles and AZ91 matrix, thermal strain easily occurs in MMCs during HPR deformation. Thermal strain also induced partial dislocations appear near TC4 particles, which ultimately contributes to the dislocation strengthening. Thirdly, load transfer strengthening also provides a certain strengthening contribution, although it is not as dominate as fine grain strengthening (approximately 6–9% of total contribution to YS). It can be seen from the tensile fracture morphology (Fig. 8b, c) that there is a good interfacial integration between the AZ91 matrix and TC4 particles when the thickness reduction is 70% and 80%, which suggests that the stress could effectively transfer from Mg matrix to TC4 particles. Besides the strengthening mechanism mentioned above, the Orowan strengthening is another important strengthening mechanism in conventional MMCs, which is caused by the obstruction when the dislocation tries to pass through these reinforcement particles [32]. In this work, the YS contribution induced by the Orowan mechanism can be ignored as compared to other strengthening proportion. The YS enhancement by Orowan is closely associated with reinforcement particles size and dispersion, indicating that the contribution through Orowan strength is inversely proportional to the increase in particles size and inter-particles spacing. Consequently, the YS enhancement by Orowan mechanism is relatively weak due to large particle size and mean spacing.

In addition to good strength properties, the HPR TC4/AZ91 composites also maintain favorable ductility after HPR. The improved ductility is mainly attributed to two aspects, i.e., grain refinement and deformable TC4 particles. Firstly, the grain refinement has a significant influence on the ductility of MMCs. The finer the grains are, the more the grains are in the

unit volume. When plastic deformation occurs, the stress can be effectively dispersed into more grains to avoid stress concentration (as depicted in Fig. 11), so as to avoid cracking and maintain better ductility [33]. Figure 4 also shows that the average grain size of TC4/AZ91 composites is significantly refined from 44 μm in sintering TC4/AZ91 composites to 32.87 μm, 7.75 μm and 9.78 μm after HPR deformation, which is greatly beneficial to improve the ductility of composites. Secondly, compared with traditional ceramic particles, TC4 particles have deformability. Wang et al. confirmed that deformable TC4 particles can effectively reduce the stress concentration in matrix around them and thus improve the ductility of the alloys [10]. Ye et al. demonstrated that micro-Ti particle-reinforced Mg alloys can achieve favorable strength while maintaining good ductility [34]. The reason is that the grains around the TC4 particles are refined and form nanoscale interface products, which is conducive to delay interfacial cracking to contribute to good ductility. In this work, the favorable ductility obtained through HPR deformation is mainly due to the refined grains around TC4 particles and the formation of a good interfacial bonding with them to avoid stress concentration leading to cracking.

Conclusions

In this work, the TC4/AZ91 composites fabricated through spark plasma sintering (SPS) followed by hard plate rolling (HPR) show favorable strength and ductility. Through the microstructure analysis and mechanical test, the main conclusions are as follows:

1. TC4 particles induce dynamic recrystallization by PSN mechanism, and the Zener pinning of precipitated $Mg_{17}Al_{12}$ jointly promotes grain refinement during HPR deformation. The finer the grain size is, the favorable interfacial bonding will be between TC4 particles and AZ91 matrix.
2. The deformability of TC4 particles is beneficial to relax stress concentration near them during HPR, resulting in slightly smaller grain sizes near TC4 particles than those away from ones.
3. The HPR TC4/AZ91 composite with ~70% thickness reduction not only shows favorable strength (YS and UTS are 206 Mpa and 349 Mpa, respectively) but also achieves good elongation (EL = 7.9%). The excellent mechanical properties are mainly ascribed to grain refinement, the deformability of TC4 particles and the good interface bonding between TC4 particles and AZ91 matrix.

Acknowledgements

All people who have contributed to this work have included in the author list. And, the financial funding supported by Northwest Institute For Non-ferrous Metal Research (YK2021-1/ZZML-2201).

Author contributions

XC was involved in conceptualization, methodology, investigation, validation, resources, supervision and writing—reviewing and editing. BW was responsible for methodology, investigation and validation. ML took part in methodology, project administration and funding acquisition. JL participated in investigation and validation.

Data and code availability

Not applicable.

Declarations

Conflicts of interest There are no actual or potential conflicts of interest that have appeared to influence the work reported in this paper.

Ethical approval Not applicable.

Supplementary information This section mainly includes some unimportant information in the manuscript including the size of the raw powder and some chemical reagent components, with the aim of increasing its completeness.

Supplementary Information The online version contains supplementary material available at https://doi.org/10.1007/s10853-023-09044-8.

References

[1] Prasad SVS, Prasad SB, Verma K, Mishra RK, Kumar V, Singh S (2021) The role and significance of magnesium in modern day research-a review. J Magn Alloy 10(1):1–61

[2] Song JF, She J, Chen DL, Pan FS (2020) Latest research advances on magnesium and magnesium alloys worldwide. J Magn Alloy 8:1–41

[3] Dong YP, Tang JC, Wang DW, Wang N, He ZD, Li J, Zhao DP, Yan M (2020) Additive manufacturing of pure Ti with superior mechanical performance, low cost, and biocompatibility for potential replacement of Ti-6Al-4V. Mater Des 196:109142

[4] Hu M, Wei S, Shi Q, Ji Z, Xu H, Wang Y (2020) Dynamic recrystallization behavior and mechanical properties of bimodal scale Al_2O_3 reinforced AZ31 composites by soild state synthesis. J Magn Alloy 8(3):841–848

[5] Singh N, Belokar RM (2021) Tribological behavior of aluminum and magnesium-based hybrid metal matrix composites: a state-of-art review. Mater Today Proc 44:460–466

[6] Wang XJ, Wang NZ, Wang LY, Hu XS, Wu K, Wang YQ, Huang YD (2014) Processing, microstructure and mechanical properties of micro-SiC particles reinforced magnesium matrix composites fabricated by stir casting assisted by ultrasonic treat. Mater Design 57:638–645

[7] Xiao P, Gao YM, Xu FX, Yang SS, Li YF, Li B, Zhao SY (2019) Hot deformation behavior of in-situ nanosized TiB2 particulate reinforced AZ91 Mg matrix composite. J Alloy Compd 798:1–11

[8] Zhang B, Yang CL, Li HX, Sun YX, Yan YZ, Zhao TH, Li XL, Liu F (2020) Achieving high strength-ductility combination and negligible yield asymmetry in extruded AlN/AZ91 composite rods. Mater Sci Eng A 773:138842

[9] Wang BJ, Xu DK, Wang SD, Sheng LY, Zeng RC, Han EH (2019) Influence of solution treatment on the corrosion fatigue behavior of an as-forged Mg-Zn-Y-Zr alloy. Int J Fatigue 120:46–55

[10] Wang X, Wang X, Hu X, Wu K (2020) Effects of hot extrusion on microstructure and mechanical properties of Mg matrix composite reinforced with deformable TC4 particles. J Magn Alloy 8(2):421–430

[11] Zhu S, Luo T, Zhang T, Li Y, Yang Y (2017) Effects of Cu addition on the microstructure and mechanical properties of as-cast and heat-treated Mg-6Zn-4Al magnesium alloy. Mater Sci Eng A 689:203–211

[12] Kim JI, Nguyen HN, You BS, Kim YM (2019) Effect of Y addition on removal of Fe impurity from magnesium alloys. Scripta Mater 162:355–360

[13] Rashad M, Pan F, Asif M, She J, Ullah A (2015) Improved mechanical proprieties of "magnesium-based composites" with titanium-aluminum hybrids. J Magn Alloy 3:1–9

[14] Yu H, Zhou H, Sun Y, Ren L, Wan Z, Hu L (2018) Microstructures and mechanical properties of ultrafine-grained Ti/AZ31 magnesium matrix composite prepared by powder metallurgy. Adv Powder Technol 29(12):3241–3249

[15] Rashad M, Pan F, Tang A, Lu Y, Asif M, Hussain S, She J, Gou J, Mao J (2013) Effect of graphene nanoplatelets (GNPs) addition on strength and ductility of magnesium titanium alloys. J Magn Alloy 1(3):242–248

[16] Huang G, Shen Y (2017) The effects of processing environments on the microstructure and mechanical properties of the Ti/5083Al composites produced by friction stir processing. J Manuf Process 30:361–373

[17] Roy S, Kannan G, Suwas S, Surappa MK (2015) Effect of extrusion ratio on the microstructure, texture and mechanical properties of $(Mg/AZ91)_m$-SiC_p composite. Mater Sci Eng A 624:279–290

[18] Dinaharan I, Zhang S, Chen G, Shi Q (2020) Titanium particulate reinforced AZ31 magnesium matrix composites with improved ductility prepared using friction stir processing. Mater Sci Eng A 772:138793

[19] Wang HY, Yu ZP, Zhang L, Liu CG, Zha M, Wang C, Jiang QC (2015) Achieving high strength and high ductility in magnesium alloy using hard-plate rolling (HPR) process. Sci Rep 5:17100

[20] Yu H, Sun Y, Wan Z, Zhou H, Hu L (2018) Nanocrystalline Ti/AZ61 magnesium matrix composite: evolution of microstructure and mechanical property during annealing treatment. J Alloy Compd 741:231–239

[21] Wang XJ, Wu K, Zhang HF, Huang WX, Chang H, Gan WM, Zheng MY, Peng DL (2007) Effect of hot extrusion on the microstructure of a particulate reinforced magnesium matrix composite. Mater Sci Eng A 465:78–84

[22] Xiang SL, Gupta M, Wang XJ, Wang LD, Hu XS, Wu K (2017) Enhanced overall strength and ductility of magnesium matrix composites by low content of graphene nanoplatelets. Compos A 100:183–193

[23] Luo H, Li JH, Ye JL, Lu YF, Tan J, Song JF, Chen XH, Zheng KH, Pan FS (2022) Influence of Ti-6Al-4V particles on the interfacial microstructure and strength-ductility synergetic mechanism of AZ91 magnesium alloy. Mater Charact 191:112154

[24] Yu Z, Tang A, Zhang L, Pan F (2014) Effect of microalloying with titanium on microstructure and mechanical properties of AZ91 magnesium alloy. Mater Sci Technol 30:1441–1446

[25] Chua BW, Lu L, Lai MO (1999) Influence of SiC particles on mechanical properties of Mg based composite. Compos Struct 47:595–601

[26] Deng KK, Wu K, Wu YW, Nie KB, Zheng MY (2010) Effect of submicron size SiC particulates on microstructure and mechanical properties of AZ91 magnesium matrix composites. J Alloy Compd 504:542–547

[27] Xiao P, Gao YM, Yang CC, Liu ZW, Li YF, Xu FX (2018) Microstructure, mechanical properties and strengthening mechanisms of Mg matrix composites reinforced with in situ nanosized TiB_2 particles. Mater Sci Eng A 710:251–259

[28] Robson JD, Henry DT, Davis B (2009) A new class of metrics for the macroscopic crystallographic space of grain boundaries. Acta Mater 57(9):2739–2747

[29] Liu L, Zhou X, Yu S, Zhang J, Lu X, Shu X, Su Z (2020) Effects of heat treatment on mechanical properties of an extruded Mg-4.3Gd-3.2Y-1.2Zn-0.5Zr alloy and establishment of its Hall-Petch relation. J Magn Alloy 10(2):501–512

[30] Chen LY, Xu JQ, Choi H, Pozuelo M, Ma X, Bhowmick S, Yang JM, Mathaudhu S, Li XC (2015) Processing and properties of magnesium containing a dense uniform dispersion of nanoparticles. Nature 528:539–543

[31] Chelliah NM, Singh H, Raj R, Surappa MK (2017) Processing, microstructural evolution and strength properties of in-situ magnesium matrix composites containing nano-sized polymer derived SiCNO particles. Mater Sci Eng A 685:429–438

[32] Rashad M, Pan F, Asif M (2016) Exploring mechanical behavior of Mg–6Zn alloy reinforced with graphene nano-platelets. Mater Sci Eng A 649:263–269

[33] Vahedi F, Zarei-Hanzaki A, Salandari-Rabori A, Abedi HR, Razaghian A, Minarik P (2020) Microstructural evolution and mechanical properties of thermomechanically processed AZ31 magnesium alloy reinforced by micrographite and nano-graphene particles. J Alloys Compd 815:152231

[34] Ye JL, Li JB, Luo H, Tan J, Chen XH, Feng B, Zheng KH, Pan FS (2022) Effect of micron-Ti particles on microstructure and mechanical properties of Mg-3Al-1Zn based composites. Mater Sci Eng A 833:142526